Anisotropy of momentum distributions in atomic-collision cascades generated in fcc materials

M. Hou
Université Libre de Bruxelles, CP234, Bd du Triomphe, B-1050 Brussels, Belgium

W. Eckstein
Max-Planck Institut für Plasmaphysik—EURATOM Association, D-8046 Garching, Federal Republic of Germany
(Received 4 December 1989)

The distributions of particle momentum directions in atomic-collision cascades are studied by means of computer simulation with the MARLOWE program. In contrast to the random model, the atomic-collision cascade development in single crystals is found to be complex and governed by the lattice crystallography. In addition to the well-known one-dimensional focusing effects, two-dimensional transient focusing is found to play an important role in the cascade development. Unstable one-dimensional focusing of trajectory segments also makes a large contribution to the momentum direction distributions at various stages of the cascade generation. Large thermal displacements of lattice atoms are not found to randomize the cascades. They may, however, induce anisotropy characteristics in momentum direction distributions different from those calculated for a static lattice.

I. INTRODUCTION

Several analytical theories make use of a random cascade model.[1-4] Despite strong assumptions inherent to this model, it allows useful predictions for dense materials, e.g., on the basis of linearized transport equations in a Boltzmann gas.[4]

One of the basic assumptions is that of the material is isotropic with the consequence that at each collision step all possible collision impacts are equally probable. It is then assumed that atoms are randomly distributed in the material, and that the scattering probability conforms to Poisson statistics.[5] The assumption of target isotropy is still used in quite recent work.[6-8] The development of collision cascades in single crystals or polycrystals, however, is a frequent experimental situation. The influence of the crystal lattice on the atomic motion has given rise to the study of several processes: channeling of the primary ions when incident in suitable directions,[9,10] influence of channeling on sputtering yields,[11] focused collision sequences in collision cascades,[12-15] and also possible channeling of secondary recoils[16] and its influence on subcascade formation.[17] Since the length of focusing chains is usually rather short, they have been considered to have no major effect on many collision cascade characteristics. One exception is the angular distribution of atoms sputtered from single crystals, which is known to be anisotropic.[18] This has generally been attributed to atomic ejection in low-index crystallographic directions by nascent focusing[19] or stably focused collision chains.[15] The relative contribution of such correlated events to sputtering in preferential directions was recently discussed in the binary-collision approximation.[20,21]

Computer simulation methods allows one to avoid several assumptions required to develop an analytical theory and have already been used to study sputtering from single crystals[22] and the spatial configuration of atomic displacements.[17,23,24] Aspects of momentum distributions in collision cascades recently were emphasized which do not account for the effects of the lattice ordering.[25,26] A first study of these effects on momentum fluxes is presented in Ref. 27.

The purpose of the present work is to investigate the strong anisotropy of momentum distributions in single-crystal structures as well as their dependence on the kinetic energy of the cascade atoms. This is done by computer simulation. It is shown that the lattice structure of the solid acts as a constraint that governs the anisotropy of momentum distributions, which is complex in detail. This represents a major difference between the evolution of collision cascades in single crystals and polycrystals on the one hand and random materials on the other.

In addition to the focusing processes quoted above, various kinds of unstable and hence transient focusing processes take place. Their description will demonstrate the basic role of the crystal lattice and will show how they may dominate the cascade development.

The discussion is based on the case study of low-energy irradiation of gold (111) surfaces with heavy atoms. Elastic energy transfer thus represents the dominant energy-loss mechanism. Results similar to those discussed below were obtained with copper targets as well as with (100) and (110) surfaces and with different projectile masses and energies. In the case of higher-energy beams, short collision sequences are generally enough to reach energies per moving atom of the order of those considered here, suggesting that the present case study is representative of many practical situations. The discussion is intentionally limited to the major characteristics of the cascade development, although complexity in closer details is shown. Its approach requires another investigation method.

II. THE SIMULATION MODEL

The calculations were made with the MARLOWE computer simulation code.[28] We had already used it for sputtering calculations,[20,29] and comparison with experiment had allowed us to adjust the model parameters reasonably well. The same parameters are used in the present calculations. The discussion is based on the example of cascades generated in gold single crystals by incident high-energy xenon atoms.

The MARLOWE code is based on the binary-collision approximation. The atomic collisions are governed by the pairwise Molière potential[30] with the screening length for gold suggested by Robinson.[28] Firsov screening distances[31] are assumed to be valid for rare-gas atoms, and those for heteronuclear pairs (Xe-Au) are estimated as harmonic means of the screening lengths for the homonuclear pairs.[32]

Between collisions, particles are assumed to move along their asymptotic trajectories. Provision is made for an approximate treatment of quasisimultaneous collisions. The binding energy of the gold atoms to their lattice sites is taken as zero. A small binding energy, however, is assumed for replacement collisions (0.2 eV) in order to correct for the many-body nature of such events as discussed in detail on the basis of comparison with classical dynamics calculations.[22] The choice of 0.2 eV is somewhat arbitrary. As shown in Ref. 22, the mean energy loss along replacement sequences is systematically underestimated because of the approximate treatment of quasisimultaneous events in the binary-collision approximation. To our knowledge, no information about the magnitude of this underestimate is available in the case of gold. The energy dissipation due to binary collisions proceeds until the kinetic energy of the moving particles drops below a preset cutoff value, which is also used as an energy displacement threshold (3.78 eV). Only the contributions of collisions with an impact parameter smaller than 0.62 a_0 (where a_0 is the length of a lattice cell edge) are considered. Inelastic energy loss is assumed to be equally shared between local and nonlocal electron excitation according to Oen and Robinson[33] and Lindhard,[34] respectively.

Time is not a currently available cascade characteristic in the present version of the code (version 12). Temporal aspects of collision cascades are given in.[35] Real time is also used in simulating sputtering of silver by bismuth atoms and of carbon by very large argon clusters.[36] It was also introduced in MARLOWE for the study of Auger emission[37] as a descriptive parameter whose range of application is limited to the high-energy part of the cascades. In the present version of the MARLOWE code, the fastest atom after each collision step is selected as the next projectile to be followed, until all cascade particles have their kinetic energy below the cutoff value. Some minor atom permutations may occur that are typical of hashing algorithms as used here in order to speed up the cascade calculations.

The present work focuses on the dependence of the angular distribution of the atomic motion on the kinetic energy of the moving atoms. Such angular distributions are recorded for all particles entering a prespecified kinetic energy interval. In such a way, the atomic motion can be analyzed within specified energy intervals, irrespective of the time evolution. Consecutive energy intervals are taken as $(E_0/2^n, E_0/2^{n+1})$, where E_0 is the primary energy for increasing integer values of n until the cutoff energy is reached. The number of cascades that had to be generated in order to obtain relevant statistics in the momentum direction distributions within a resolution of 0.42×10^{-3} sr was typically of the order of a hundred thousand.

III. ANGULAR DISTRIBUTION OF THE ATOMIC MOTION

A. Scattering probability distributions

Statistical independence of collision events in a collision cascade is only possible if the path length between successive collisions is large with respect to the collision radius.[5] This is generally not the case in solids and the question is to identify how large the deviations from the random cascade model are.

A first approach may be made on the basis of scattering probability distributions. As far as simulated cascades are concerned, such distributions are easily obtained by scoring the collision frequencies as a function of the impact parameter squared. This is shown in Fig. 1, were the cases of amorphous, polycrystalline, and crystalline gold targets are compared with the uniform distribu-

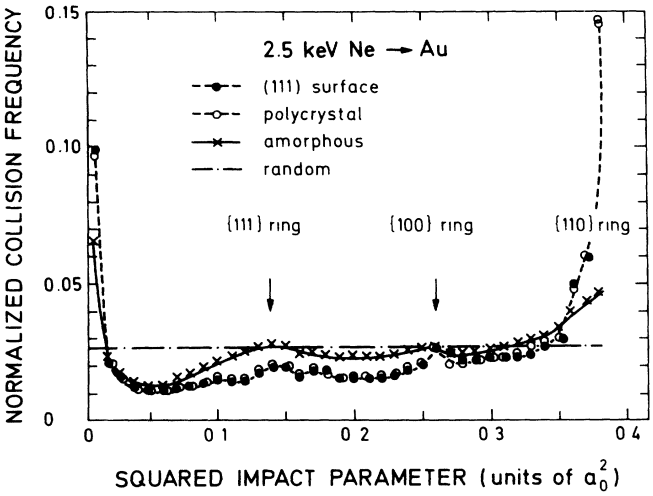

FIG. 1. Impact parameter squared distributions for collision cascades generated by 2.5 keV neon atoms at normal incidence on a gold target. The results obtained by simulation in the case of a single crystal with a {111} surface, of a polycrystal and of an amorphous target are compared with the uniform distribution associated with a random target model. The arrows indicate the impact parameter squared for the simultaneous interaction between a projectile and a ring of lattice atoms in {111}, {110}, and {100} planes, when the trajectories pass through the center. All collisions are considered in this distribution, involving impact parameters smaller than 0.6 a_0, where a_0 is the length of the lattice cell edge unit. The {110} ring appears at an impact parameter squared $b^2=0.375\ a_0^2$.

tion of a random cascade model. The computer results indicate that structures occur in the impact parameter distributions that correspond to head-on collisions as in focusing chains and the associated interaction with rings of atoms in the {111}, {100}, and {110} planes. The structures are identical in the single-crystal and polycrystal cases, showing that the influence of the incidence conditions on the collision probability distribution in a cascade is small. It should be noted that the short-range structure in the amorphous model material has a significant influence on the collision statistics. The sharp peaks observed for polycrystals and single crystals at close-to-zero impact parameters and associated to {110} rings reflect the efficiency of assisted focusing in the ⟨110⟩ directions.

These impact parameter distributions may be energy dependent. On the other hand, since the impact parameter at a given energy is directly related to the scattering angle, the energy dependence of collision statistics and its dependence on energy can also be viewed in terms of momentum distributions. These allow a description of the cascade development, as shown in the next sections. Greater detail is provided in Ref. 38.

B. The energy dependence of angular distributions in the bulk

The angular distributions are constructed in a two-dimensional representation. One axis is the azimuthal angle φ with respect to a ⟨110⟩ surface direction and the other is the cosine of the angle β between the momentum direction and the inward surface normal. In such a representation, the direction distributions are constructed at a constant solid angle. The crystallographic directions required for the discussion below as well as the loci of the directions parallel to the major crystallographic planes are represented in Fig. 2.

The distributions are represented in the form of contour line plots of equal intensities. The number of contour lines is limited to 20. Their equidistance corresponds to 5% of the maximal intensity. They were constructed from direction distributions of moving atoms in all cascades. The contour lines are determined by means of an interpolation technique such that they would join boxes in the direction distributions with an equal number of counts. The data are presented for collision cascades generated in gold by 2.5-keV incident xenon projectiles.

Figure 3 shows the angular distribution of moving atoms whose kinetic energy drops below $E_0/2=1250$ eV and is in the energy interval 1250 eV to 625 eV. The distribution is highly anisotropic and, in addition to the projectile flux peaking in the forward direction, it is characterized by six major spots and minor additional structures dominated by the contribution of primary and secondary recoils. The latter are of increasing complexity as the energy gets lower and will not be analyzed in detail. According to Fig. 2, the major spots are easily identified as being associated with ⟨100⟩ ($\cos\beta=0.58$) and ⟨111⟩ ($\cos\beta=1$, $\cos\beta=0.33$) directions. ⟨111⟩ spots of lower intensity also appear in the backward direction ($\cos\beta=-0.33$), showing the momentum reversal. The energies involved in Fig. 3 are above known values for focusing thresholds[22] and, consequently, these spots cannot be attributed to focusing chains. They are better explained by a lens effect similar to that discussed in the early comments on low-energy channeling[9,39] as well as in the description of surface reflection from semichannels.[40] Indeed, an atom recoiling from a fcc lattice site, except in

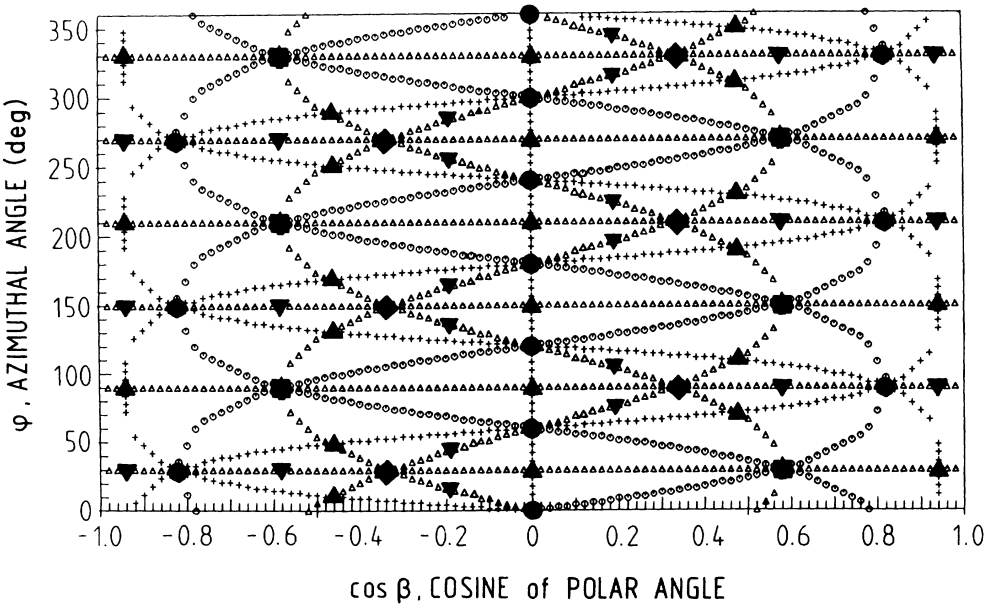

FIG. 2. Loci of the directions parallel to the most compact crystallographic planes. Their intersections represent the close-packed directions in the lattice that are labeled in the figure. ○○○: loci of directions parallel to {100} planes; △△△: loci of directions parallel to {110} planes; +++: loci of the directions parallel to the {111} planes; ■: ⟨100⟩ directions; ●: ⟨110⟩ directions; ♦: ⟨111⟩ directions; ▲ : ⟨112⟩ directions and ▼ : ⟨221⟩ directions.

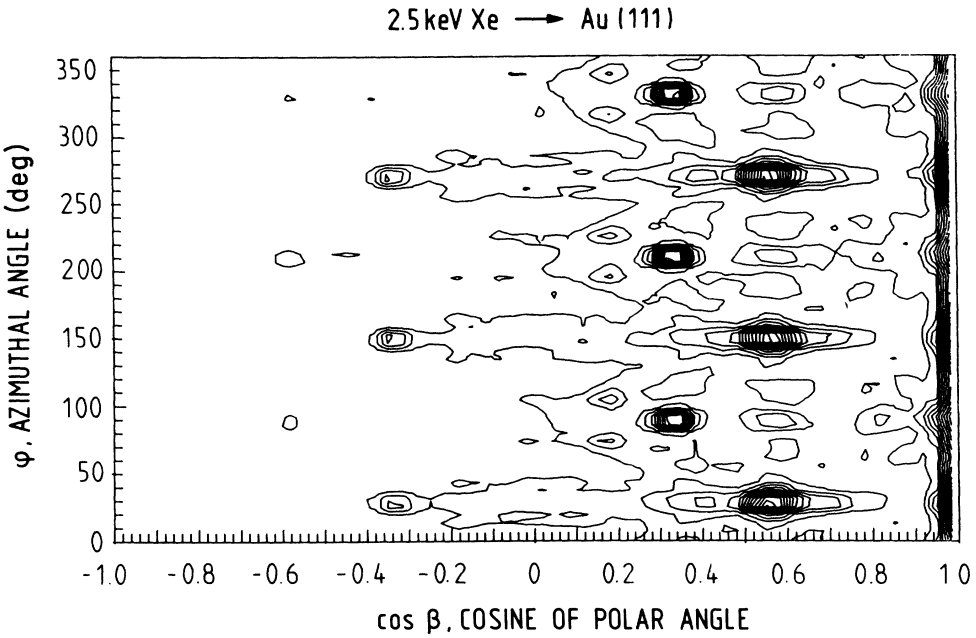

FIG. 3. Contour line plots representing the angular distributions of atoms moving in the cascades generated by 2.5 keV Xe atoms incident on a Au(111) surface. The abscissae represent the cosine of the polar angle β with respect to the inward surface normal, and the ordinates represent the azimuth φ with respect to a $\langle 110 \rangle$ surface direction. The plot is drawn for all particles whose kinetic energy falls into the interval 1250 to 625 eV. The equidistance of the 20 adjacent contour lines is 5% of the maximum intensity.

special cases, interacts primarily with a ring of atoms which tends to focus the trajectory toward its axis. Successive atoms along a $\langle 111 \rangle$ axis are fourth neighbors separated by two parallel rings each formed by three first neighbors, and the focusing effect is the strongest possible. The next strongest is along $\langle 100 \rangle$ axes. These are surrounded by rings formed by four first neighbors, with a shorter interatomic spacing along the axis (second-neighbor distance). The third strongest is along the $\langle 110 \rangle$ axes, in which successive atoms are first neighbors separated by one rather open ring of first and second neighbors. It is thus found that, owing to these rings, focusing can happen over short distances. This picture is consistent with the results in Fig. 3. The $\langle 111 \rangle$ spots are found to be the most intense, followed by $\langle 100 \rangle$ spots while none are seen in $\langle 110 \rangle$ directions. In the latter, the effect of the rings is balanced by successive close-impact collisions along the axes, which, at such high energies tends to defocus the beams. The $\langle 100 \rangle$ and $\langle 111 \rangle$ beams diverge as the energy per atom decreases as a result of successive collisions. Two lower-energy situations are given in Figs. 4(a) and 4(b). Taking advantage of the sixfold symmetry of the $\{111\}$ surface, one third of the full angular distribution is sufficient to get a clear picture of the whole distribution. This is what is done in Figs. 4(a) and 4(b) for atoms whose energy falls into the energy intervals 312 to 156 eV and (156 to 78 eV), respectively.

The complexity is found to be increased as compared with higher-energy situation in Fig. 3. As expected, the relative intensities of the $\langle 111 \rangle$ and $\langle 100 \rangle$ beams are lower. The angular distributions are now dominated by $\langle 110 \rangle$ beams, as a consequence of another focusing process. This one can be identified by comparing Figs. 4(a) and 4(b). The $\langle 110 \rangle$ spots (directions at $\cos\beta = -0.81$, $\cos\beta = 0.0$, $\cos\beta = 0.81$) are found to become sharper as the kinetic energy per atom decreases. Superpositioning of Figs. 2 and 4(a) would show that the steering observed in the $\langle 110 \rangle$ spots aligns perfectly with $\{110\}$ planes.

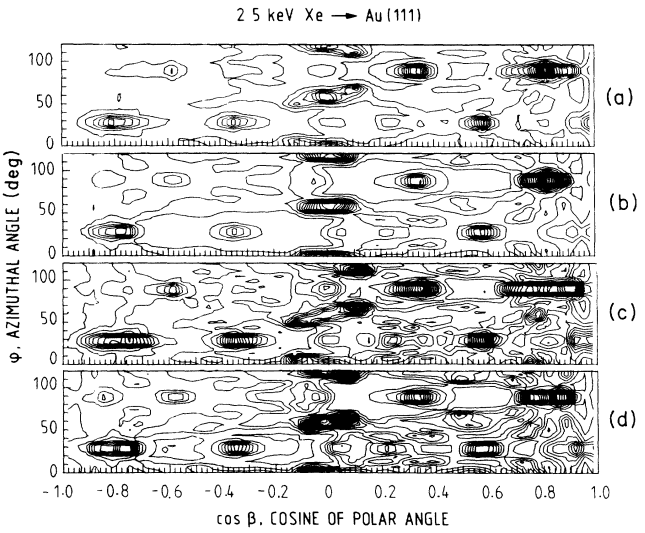

FIG. 4. Contour line plots representing the angular distributions of atoms moving in the cascades whose energy falls into the interval 312.5 to 156 eV: 4(a) and 4(c) and into the interval 156 to 78 eV: 4(b) and 4(d). Figures 4(c) and 4(d) are the same as Figs. 4(a) and 4(b), respectively, in which the contribution of replacement sequences is omitted. The azimuth range is limited to the interval $\varphi = 0°$ to $\varphi = 120°$. The equidistance of the 20 adjacent contour lines is 5% of the maximum intensity.

This family of planes plays a major role in the cascade development, which will be further emphasized. At the present stage, let us note that the major beam and steering directions found in Fig. 4 are all included in {110} planes. On the other hand, owing to the nature of the {110} planes stacking in fcc lattices ($ABAB\cdots$) particles moving in or close to their direction are subjected to opposite transverse forces which tend to feed their trajectories inside the planes, as in a potential well. In principle, the same is true of {100} planes, but their equidistance is too large to assure a similar two-dimensional focusing effect.

The transition toward one-dimensional focused ⟨110⟩ beams seen by comparing Figs. 4(a) and 4(b) can be identified as a consequence of two distinct processes: formation of replacement sequences and the low-energy channeling in the ⟨110⟩ open directions. Figures 4(c) and 4(d) represent the same direction distributions as Figs. 4(a) and 4(b) respectively, the only difference being that replacement sequences are suppressed. In Fig. 4(c), the ⟨110⟩ beams are found to be split into two parts aligning with the {110} planes. When replacement sequences are also represented, the same spots [Fig. 4(a)] are peaked in the ⟨110⟩ direction ($\cos\beta=0$), showing that they are therefore responsible. Low-energy channeling was observed both experimentally[41] and by computer simulation[40] although, at these low energies, channeling cannot be described as a sequence of independent interactions with strings of atoms.[10] In the present study, evidence of low-energy channeling is found in Fig. 4(d) in which, despite the truncation of replacement sequences, the ⟨110⟩ beams intensities are found to be quite pronounced.

When the kinetic energy of the moving cascade atoms decreases, the direction distributions still remain highly anisotropic despite the fact that, as can be seen from Fig. 5, the low-energy ⟨110⟩ channeling is unstable and partly vanishes as a result of a two-dimensional process, giving rise to a sequence of transient structures.

Figures 5(a)–5(d) represent a sequence of direction distributions in different energy intervals, the highest of them being 78 to 39 eV in Fig. 5(a) and the last of them 9.8 to 4.9 eV. The energy cutoff in the cascade development is 3.78 eV. The divergence of the very strongly focused ⟨110⟩ beams in Fig. 5(a) is clearly observed at lower energies. The loci of the directions parallel to the major plane directions is shown in Fig. 5(c) to emphasize the two-dimensional nature of the process, inside {110} planes. The configuration of the major beams at the lowest energies considered [Fig. 5(d)] corresponds to low-index crystallographic directions which are identified by comparison with Fig. 2 as ⟨110⟩, ⟨111⟩, ⟨112⟩, and ⟨221⟩. Figure 5(e) represents the same distribution as Fig. 5(c) without the contribution of replacement sequences. It shows that the (low-energy) channeled fraction of the ⟨110⟩ beams splits into two parts, one remaining stable and the other being deflected from the ⟨110⟩ toward the ⟨221⟩ neighboring directions along the {110} planes. This suggests a distinction between the best confined, and thus stable, channeled trajectories and those with larger oscillations which diverge although remaining constrained inside {110} planes. There is no reason for the ⟨221⟩ and the ⟨112⟩ beams shown in Fig. 5(d) to be stable, but further energy dissipation was not investigated. On the other hand, the energy range considered here 9.8 to 4.9 eV, is typical of about half the atoms which contribute to sputtering. These directions will be shown to be of major importance in the interpretation of sputtering patterns in a forthcoming paper.[42] It is seen in Fig. 5(d) that even those cascades not contributing to the major beams display momentum aligning with {110} planes and leaving the other directions in the distribution depleted. This illustrates the two-dimensional nature of the cascade development in fcc static single crystals.

Such peculiar behavior is a consequence of the special geometrical properties of the {110} planes. On one hand, they are not quite compact, thus allowing rather long atomic flights in them without small-impact scattering and, on the other, the equidistance is quite small (0.35 lattice units) and pairs of surrounding planes exert symmetric repulsive forces on the moving atoms. Strictly speaking however, this symmetry only occurs in a static undistorted lattice and breaks down because of thermal displacements. Their effect is moderated by correlations in the thermal motion of the lattice. However, the fate of the strong lattice constraint on the cascade development

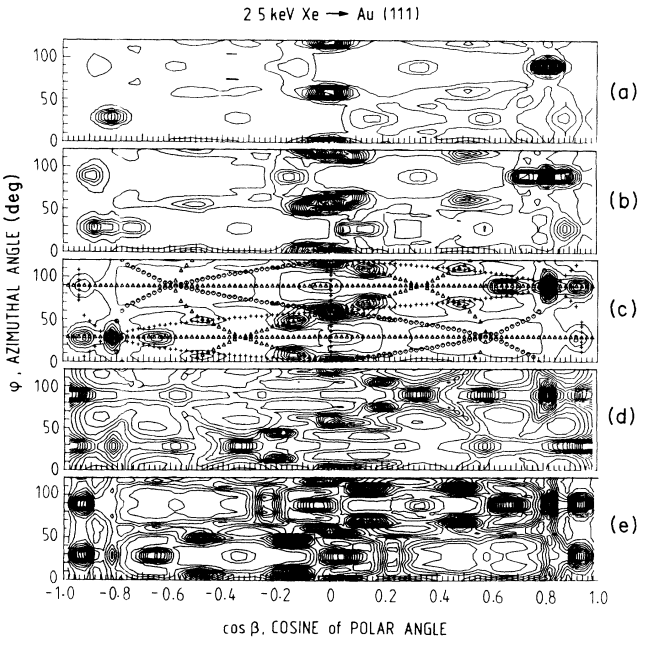

FIG. 5. Contour line plots representing the angular distributions of atoms moving in the cascades whose energy falls into the interval 78 to 39 eV: 5(a); 39 to 19.5 eV: 5(b); 19.5 to 9.75 eV: 5(c); 9.75 to 4.9 eV: 5(d). Figure 5(e) is the same as Fig. 5(c), in which the contribution of replacement sequences is omitted. In Fig. 5(c) the loci of the directions parallel to the main crystallographic planes (see Fig. 2) are represented in order to guide the eye in identifying the two-dimensional processes. The equidistance of the 20 adjacent contour lines is 5% of the maximum intensity.

in a static crystal can be influenced by thermal disorder and is analyzed in the next section.

C. Thermal displacement effects

The question of course arises whether thermal vibrations can lead to randomization of the cascade. As will be shown, the answer is negative, but the nature of the lattice constraint is greatly modified. The one- and two-dimensional focusing still remains the dominant characteristic feature of the cascades. In order to show this, the simulations were repeated, with a temperature of 600 K and uncorrelated thermal displacements, according to the Debye-Waller model.[43] Since thermal vibrations are known to be correlated, the procedure is expected to provide an overestimate of the thermal effect on the cascade development.

The results are illustrated in Fig. 6, showing the distributions obtained in various energy intervals. The contrast between the two families of anisotropies obtained with the static lattice model and with thermal displacements included is seen by, for example, comparing Fig. 6(c) and Fig. 5(a) and between Fig. 6(e) and Fig. 5(b). Figure 6(a) (625 to 312 eV) is a typical direction distribution of the high-energy cascade atoms. The same lens effect as in the static lattice case is found to focus the trajectories

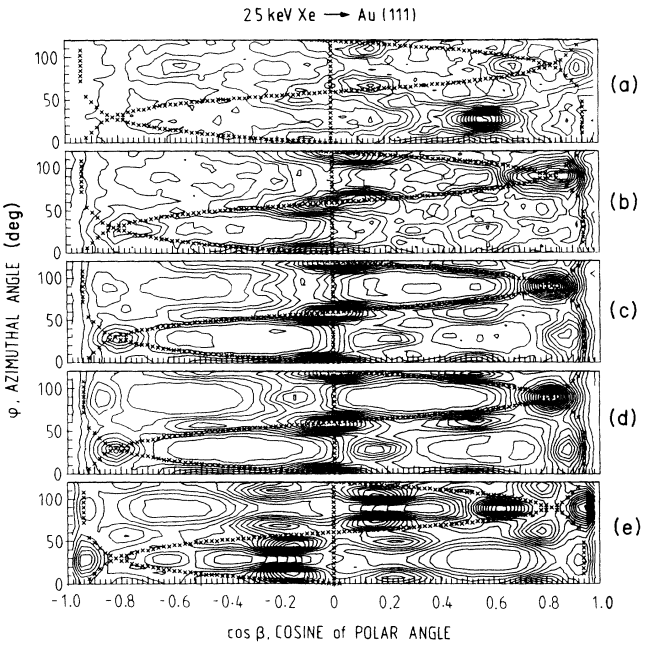

FIG. 6. Contour line plots representing the angular distributions of atoms moving in the cascades whose energy falls into the interval 625 to 312.5 eV: 6(a); 312.5 to 156 eV: 6(b); 156 to 78 eV: 6(c); 78 to 39 eV 6(d) and 19.5 to 9.75 eV: 6(e) 600 K uncorrelated thermal vibrations of gold atoms are included in the simulations. The loci of directions parallel to {111} planes is represented in order to guide the eye in identifying the two-dimensional {111} focusing effect. The equidistance of the 20 adjacent contour lines is 5% of the maximum intensity.

into ⟨100⟩ beams. As can be expected from the thermal disorder, focusing is less intense. The major difference with the high-energy distributions in a static lattice is that thermal displacements completely destroy the ⟨111⟩ spots. This is a consequence of the fact that the {111} rings are so compact that a small displacement of the atoms introduces a local perturbation of the symmetry in the potential distribution, making focusing no longer possible. At lower energies [Fig. 6(b)], ⟨110⟩ spots are found to form, again two dimensionally, but as a result of alignment with {111} planes and not with {110} ones, as in a static lattice. Forces transverse to the {110} planes are no longer symmetric and the resulting focusing effect is strongly decreased. On the other hand, {111} planes are quite compact and their equidistance rather large (0.58 lattice units). Consequently, they represent sufficiently high potential barriers in between which the atomic motion is favored. This effect, together with ⟨110⟩ replacement sequences and low-energy channeling, dominates in Fig. 6(c) (156 to 78 eV). However, at these and lower energies, additional beams appear in open directions and the relative effect of {111} planes decreases simultaneously. Because of thermal displacements, {111} planes represent locally corrugated walls, and the effect of this corrugation is to defocus the lowest energy trajectories, which are governed by individual collisions rather than by multiple correlated scattering. As a consequence, these are fed into the main open directions. Some align with the {110} planes (close to ⟨112⟩ and ⟨221⟩) but no {110} planar effect is observed. Others appear which do not align with low-index crystallographic planes. By breaking the symmetry and corrugating the compact atomic planes, thermal displacements thus have the effect of making two-dimensional focusing unstable. The lowest-energy trajectories [Fig. 6(e)] remain naturally fed into the most open directions, as in the case of a static lattice.

IV. CONCLUSION

The present work clearly shows that the anisotropy of direction distributions is complex and essentially driven by the crystal structure. This conclusion obviously applies to metallic polycrystals as well since the spatial extent of collision cascades is generally smaller than the size of the crystal grains. The distributions are not found to randomize when the kinetic energy becomes small, and random thermal displacements of the atoms from their lattice sites do not randomize the momentum direction distributions either. Except where replacement sequences are concerned, the evolution of the anisotropy is governed by unstable one- and two-dimensional short-range focusing processes. Lens effects dominate at high energies (a few hundred eV), planar effects ({110} for a static lattice and {111} if uncorrelated thermal displacements are taken into account) at intermediate energies (a few tens of eV), and feeding of trajectories into short-range open directions at low energies (a few eV).

Since this lattice-governed development of collision

cascades was found with several other simulation conditions, it can be concluded that the lattice constraint is the one which dominates the cascade development. The consequences on the sputtering mechanisms are significant and are planned to be examined elsewhere.[42]

ACKNOWLEDGMENTS

The authors are most grateful to M. T. Robinson for detailed discussion of cascade anisotropies and related problems.

[1]J. Lindhard, V. Nielsen, M. Scharff, and P. V. Thomsen, Mat. Fys. Medd. Dan. Vid. Selsk. **33**, 10 (1963).
[2]K. B. Winterbon, P. Sigmund, and J. B. Sanders, Mat. Fys. Medd. Dan. Vid. Selsk. **37**, 14 (1970).
[3]D. K. Brice and K. B. Winterbon, *Ion Implanted Ranges and Energy Deposition Distributions* (Plenum, New York, 1975).
[4]P. Sigmund, Phys. Rev. **184**, 383 (1969).
[5]See, for example, P. Sigmund, Mat. Fys. Medd. Dan. Vid. Selsk. **40**, 5 (1978).
[6]Y. T. Cheng, M. Nicolet, and W. L. Johnson, Phys. Rev. Lett. **58**, 2083 (1987).
[7]K. B. Winterbon, H. M. Urbassek, P. Sigmund, and A. Gras-Marti, Phys. Scr. **36**, 689 (1987).
[8]H. Urbassek, Nucl. Instrum. Methods B (to be published).
[9]M. T. Robinson, D. K. Holmes, and O. S. Oen, in *Le Bombardement Ionique, Théories et Applications* (CNRS, Paris, 1962), Vol. 113, p. 105.
[10]J. Lindhard, Mat. Fys. Medd. Dan. Vid. Selsk. **34**, 14 (1965).
[11]D. Onderdelinden, Can. J. Phys. **46**, 739 (1968).
[12]R. H. Silsbee, J. Appl. Phys. **28**, 1246 (1957).
[13]G. Leibfried, J. Appl. Phys. **30**, 1388 (1959).
[14]J. B. Gibson, A. N. Goland, M. Milgram, and G. H. Vineyard, Phys. Rev. **120**, 1229 (1960).
[15]R. S. Nelson, M. W. Thompson, and H. Montgomery, Philos. Mag. **7**, 1385 (1962).
[16]O. S. Oen and M. T. Robinson, Appl. Phys. Lett. **2**, 83 (1963).
[17]M. Hou, Phys. Rev. B **31**, 4178 (1985).
[18]G. K. Wehner, J. Appl. Phys. **26**, 1056 (1955); Phys. Rev. **102**, 690 (1956).
[19]C. Lehmann and P. Sigmund, Phys. Status Solidi **16**, 507 (1966).
[20]M. Hou and W. Eckstein, Nucl. Instrum. Methods B **13**, 324 (1986).
[21]Y. Yamamura and W. Takeuchi, Nucl. Instrum. Methods B **29**, 461 (1987).
[22]M. T. Robinson, in *Sputtering by Particle Bombardment, Physics and Applications,* edited by Behrisch (Springer, Berlin, 1981).
[23]L. Heinisch, J. Nucl. Mater. **103/104**, 1325 (1981).
[24]R. Dierckx, J. Nucl. Mater. **144**, 214 (1987).
[25]W. Eckstein and W. Möller, Nucl. Instrum. Methods B **7&8**, 727 (1985).
[26]H. J. Whitlow and M. Hautala, Nucl. Instrum. Methods B **18**, 370 (1987).
[27]H. J. Whitlow and M. Hautala, Nucl. Instrum. Methods B **6**, 466 (1985); M. Hautala and J. Likonen, Phys. Lett. A **131**, 47 (1988).
[28]M. T. Robinson and I. Torrens, Phys. Rev. B **9**, 5008 (1974).
[29]W. Eckstein and M. Hou, Nucl. Instrum. Methods B **31**, 386 (1988).
[30]G. Molière, Z. Naturforsch. **2a**, 133 (1947).
[31]O. B. Firsov, Zh. Eksp. Teor. Fiz. **33**, 696 (1958) [Sov. Phys.-JETP **6**, 534 (1958)].
[32]F. Smith, Phys. Rev. A **5**, 1708 (1972).
[33]O. S. Oen and M. T. Robinson, Nucl. Instrum. Methods **132**, 647 (1976).
[34]J. Lindhard, M. Scharff, and H. E. Schiott, Mat. Fys. Medd. Dan. Vid. Selsk. **40**, 5 (1978).
[35]M. T. Robinson, Phys. Rev. B **40**, 10 717 (1989); Nucl. Instrum. Methods B **48**, 408 (1990).
[36]Y. Yamamura, Nucl. Instrum. Methods **194**, 515 (1982); B **33**, 493 (1988).
[37]M. Hou, C. Benazeth, N. Benazeth, and C. Mayoral, Nucl. Instrum. Methods B **13**, 645 (1986); M. Hou, C. Benazeth, and N. Benazeth; Phys. Rev. A **36**, 591 (1987); C. Benazeth, M. Hou, C. Mayoral, and N. Benazeth, Nucl. Instrum. Methods B **18**, 555 (1987).
[38]M. Hou and W. Eckstein (unpublished).
[39]C. Lehmann and G. Leibfried, J. Appl Phys. **34**, 2821 (1963).
[40]M. Hou and M. T. Robinson, Nucl. Instrum. Methods **132**, 641 (1976).
[41]E. V. Kornelsen and A. A. Van Gorkum, Nucl. Instrum. Methods **170**, 161 (1980).
[42]W. Eckstein and M. Hou, Nucl. Instrum. Methods (to be published).
[43]Ch. Kittel, *Introduction to Solid State Physics,* 3rd ed. (Wiley, New York, 1968), p. 70; M. Blackman, *Handbuch der Physik,* edited by S. Flügge (Springer, Berlin, 1955), Part 1, Vol. VII, p. 377.